PHYSICAL REVIEW D **82,** 014022 (2010)

Gluon saturation and inclusive hadron production at LHC

Eugene Levin[1,2] and Amir H. Rezaeian[1]

[1]*Departamento de Física, Universidad Técnica Federico Santa María, Avenida España 1680, Casilla 110-V, Valparaiso, Chile*
[2]*Department of Particle Physics, Tel Aviv University, P.O. Box 39040, Tel Aviv 69978, Israel*

(Received 7 May 2010; published 30 July 2010)

In high-density QCD the hadron production stems from decay of mini jets that have the transverse momenta of the order of the saturation scale. It is shown in this paper that this idea is able to describe in a unique fashion both the inclusive hadron production for $\sqrt{s} \geq 546$ GeV including the first data from LHC and the deep inelastic scattering at HERA. Recently reported data from ALICE, CMS, and ATLAS including inclusive charged-hadron transverse momentum and multiplicity distribution in pp collisions are well described in our approach. We provide predictions for the upcoming LHC measurements.

DOI: 10.1103/PhysRevD.82.014022 PACS numbers: 13.60.Hb

I. INTRODUCTION

The first LHC data [1–4] on inclusive hadron production call for a theoretical understanding of these processes based on QCD. At first sight the inclusive hadron production is a typical process that occurs at long distances where one has to use the nonperturbative methods of QCD. Therefore, the field of long distance processes seems to be a relevant subject to the domain of high-energy phenomenology with the main ingredients soft Pomeron and secondary Reggeons. Such phenomenology is able to describe inclusive hadron production data (see Ref. [5] and references therein) but cannot be considered satisfactory since both soft Pomerons and Reggeons cannot be explained in terms of QCD ingredients, quarks and gluons. It should be also mentioned that the increase with energy of the average transverse momentum of the produced hadron observed experimentally [2,3] cannot be explained in the Reggeon approach.

However, high-density QCD [6–12] leads to a completely different picture of inclusive hadron production. In this approach the system of parton (gluons) at high energy forms a new state of matter color glass condensate (CGC). In the CGC picture, at high energy the density of partons ρ_p, with the typical transverse momenta less than Q_s, reaches a maximum value $\rho_p \propto 1/\alpha_s \gg 1$ (α_s is the strong-coupling constant). Q_s is the new momentum scale (saturation momentum) that increases with energy. At high energies/small Bjorken-x $Q_s \gg \mu$, where μ is the scale of soft interaction. Therefore, $\alpha_s(Q_s) \ll 1$, and this fact allows us to treat this system on solid theoretical basis. On the other hand, even though the strong-coupling α_s becomes small due to the high density of partons, saturation effects, the fields interact strongly because of the classical coherence. This leads to a new regime of QCD with nonlinear features which cannot be investigated in a more traditional perturbative approach.

In the framework of the CGC approach, the secondary hadrons are originated from the decay of gluon minijets with the transverse momentum equal to the saturation scale $Q_s(x)$. The first stage of this process is under theoretical control and determines the main characteristics of the hadron production, especially as far as energy, rapidity, and transverse-momentum dependence are concerned. The jet decay, unfortunately, could be treated mostly phenomenologically. However, we can hope that the phenomenological uncertainties would be reduced to several constants whose values will be extracted from the experiment.

Actually, such a description has passed the first check with the experimental data: the Kharzeev-Levin-Nardi (KLN) paper [13] explains the main features of inclusive hadron production in heavy-ion ion and hadron ion as well as proton-proton collisions [14] at Relativistic Heavy Ion Collider (RHIC). In this paper, we wish to improve the KLN approach by introducing two new elements, the probability to find gluon with fixed transverse momentum that describes the deep inelastic scattering (DIS) data and that satisfies the Balitsky-Kovchegov [9,11] nonlinear equation and a different description of inclusive hadron production at low transverse momenta of gluons. Overall success of our description indicates universality of the saturation physics which can be further tested at LHC and in future collider experiment.

In the next section, we discuss the k_t factorization and main formulas that we use. In particular, we consider the interrelation between the color-dipole scattering amplitude and the unintegrated gluon density that follows from the recent development of high-density QCD [15]. An important improvement here to the previous works based on the KLN approach is the explicit inclusion of the impact-parameter dependence of the saturation scale. Section III is devoted to comparison with the experimental data and to discussion of various predictions for higher LHC energies. As a conclusion, in Sec. IV, we highlight our main results and predictions for LHC.

II. INCLUSIVE GLUON PRODUCTION IN HIGH-DENSITY QCD

The gluon jet production in hadron-hadron collisions can be described by k_t factorization given by [15]

$$\frac{d\sigma}{dyd^2p_T} = \frac{2\alpha_s}{C_F}\frac{1}{p_T^2}\int d^2\vec{k}_T \phi_G^{h_1}(x_1;\vec{k}_T)\phi_G^{h_2}(x_2;\vec{p}_T-\vec{k}_T), \tag{1}$$

where $x_{1,2} = (p_T/\sqrt{s})e^{\pm y}$, and p_T and y are the transverse momentum and rapidity of the produced gluon jet. $\phi_G^{h_i}$ are the probability to find a gluon that carries x_i fraction of energy with k_T transverse momentum, and $C_F = (N_c^2 - 1)/2N_c$ is the $SU(N_c)$ Casimir operator in the fundamental representation with the number of colors equals N_c.

For a proof of k_t factorization see Ref. [15] and also Refs. [16–20] which confirm the former proof.[1] We need to recall that the proof for the k_t factorization was given for the scattering of a diluted system of partons, say for virtual photon, with a dense one. Our main idea is that we have gluon saturation for proton-proton scattering, or, in other words, we are dealing with interactions of two dense systems of partons (gluons). Therefore, the k_t factorization has to be considered here as an assumption. It should be noticed that the proof given in Refs. [15–20] shows that the k_t factorization is valid in the situation where two scales of hardness, the transverse momentum of the produced gluon (p_T) and the saturation scale, are both larger than the scale of the soft interaction (μ). For dense-dense system scattering, we have actually three scales, p_T and two saturation scales. However, only for the kinematic region where both x_1 and x_2 are small, and for p_T which is smaller than both saturation scales, we have to make an assumption about k_t factorization. In other cases in which one of the saturation scales is small, we are dealing with diluted-dense system scattering. We believe that the k_T factorization is currently the best tool at our disposal for the processes considered in this paper.

The unintegrated gluon-density $\phi_G^{h_i}(x_1;\vec{k}_T)$ and color-dipole–proton forward scattering amplitude $N(x_i, r_T; b)$ are related in a very specific way [15]. This relation reads as follows

$$\phi_G^{h_i}(x_i;\vec{k}_T) = \frac{1}{\alpha_s}\frac{C_F}{(2\pi)^3}\int d^2\vec{b}d^2\vec{r}_T e^{i\vec{k}_T\cdot\vec{r}_T}\nabla_T^2 \times N_G^{h_i}(y_i = \ln(1/x_i); r_T; b), \tag{2}$$

with

$$N_G^{h_i}(y_i = \ln(1/x_i); r_T; b) = 2N(y_i = \ln(1/x_i); r_T; b) - N^2(y_i = \ln(1/x_i); r_T; b), \tag{3}$$

where $N_G^{h_i}(y_i = \ln(1/x_i); r_T; b)$ is the dipole-hadron (h_i) forward scattering amplitude which satisfies the Balitsky-Kovchegov equation. In the above, r_T denotes the transverse dipole size and $\vec{b}$ is the impact parameter of the scattering.

Equation (3) looks very natural at large N_c. Indeed, for the color-dipole amplitude in the Glauber form $N = 1 - \exp(-\Omega/2)$ (Ω is the opacity), Eq. (3) leads to $N_G = 1 - \exp(-\Omega)$ as it should be for the scattering of the two dipoles of the same sizes. We recall that a colorless gluon probe just creates such two quark-antiquark dipoles, and the N_G is directly related to the gluon density.

Substituting Eq. (2) in Eq. (1), and after analytically performing some integrals, we obtain [15]

$$\frac{d\sigma}{dyd^2p_T}\frac{2C_F}{\alpha_s(2\pi)^4}\frac{1}{p_T^2}\int d^2\vec{b}d^2\vec{B}d^2\vec{r}_T e^{i\vec{k}_T\cdot\vec{r}_T}\nabla_T^2 \times N_G^{h_1}(y_1 = \ln(1/x_1); r_T; b)\nabla_T^2 \times N_G^{h_2}(y_2 = \ln(1/x_2); r_T; |\vec{b}-\vec{B}|). \tag{4}$$

In the above equation, $\vec{B}$ is the impact parameter between center of two hadrons, and $\vec{b}$ is the impact parameter of the produced minijet from the center of the hadron, see Fig. 1.

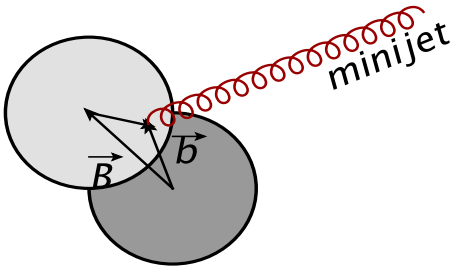

FIG. 1 (color online). Minijet production in hadron-hadron collisions in the transverse plane. The impact parameter between two hadrons is $\vec{B}$.

A. Choice of color dipole scattering amplitude

As can be seen from Eqs. (2) and (4), we need here an impact-parameter dependent color-dipole forward amplitude. We will show later that the inclusion of the impact parameter is very important in our approach and should not be ignored. The dipole-proton forward scattering amplitude $N(Y; r; b)$ (with $Y = \ln(1/x)$) can be in principle found by solving the perturbative nonlinear small-x Balitsky-Kovchegov (BK) [9,11] or Jalilian-Marian-Iancu-McLerran-Weigert-Leonidov-Kovner [12] quantum evolution equations. Unfortunately, numerical solution to these nonlinear equations in the presence of the impact parameter is very challenging [23] and is not yet available. Moreover, a numerical solution does not give us the full control on the phenomenological parameters that have been used, and we certainly lose the transparency and simplicity of physical interpretation if we rely only on the numerical solutions. Therefore, we choose a different

[1]Reference [21] states that Eq. (1) is not correct. Unfortunately, there are no discussions in the paper regarding why their result is so different from the other published papers. However, Braun has recently shown that Ref. [21] actually leads to the k_t factorization [22].

approach to the solution of the BK equation that was suggested in Ref. [24]. First, we recall that the BK equation predicts the geometric-scaling behavior [25], namely, the amplitude $N(Y;r;b)$ is not a function of three variables but it is a function of only one variable $\mathcal{Z}^2 = r^2 Q_s^2(x;b)$ ($N(Y;r;b) = F(\mathcal{Z})$), where $Q_s(x;b)$ is the saturation momentum.[2] We also know [26] the behavior of the scattering amplitude deeply in the saturation region ($\mathcal{Z} \gg 1$)

$$N(Y;r;b) = 1 - \exp\left(-\frac{\chi(\gamma_{cr})}{2(1-\gamma_{cr})}\ln^2 \mathcal{Z}\right), \quad (5)$$

where $\chi(\gamma)$ is the Balitsky-Fadin-Kuraev-Lipatov (BFKL) kernel

$$\omega(\gamma) = \bar{\alpha}_s \chi(\gamma) = \bar{\alpha}_s\{2\psi(1) - \psi(\gamma) - \psi(1-\gamma)\}, \quad (6)$$

with a notation $\bar{\alpha}_s = \alpha_s N_c/\pi$. In the above, we define $\psi(x) = d\ln\Gamma(x)/dx$ and $\Gamma(x)$ is the Euler function. The parameter γ_{cr} is the solution to the following equation:

$$\frac{d\chi(\gamma_{cr})}{d\gamma_{cr}} = -\frac{\chi(\gamma_{cr})}{1-\gamma_{cr}}. \quad (7)$$

In Ref. [26], a solution was found for the entire kinematic region for a simplified BFKL kernel, namely, instead of Eq. (6), the following kernel was used:

$$\omega(\gamma) = \bar{\alpha}_s \begin{cases} \frac{1}{\gamma} & \text{for } \mathcal{Z} = rQ_s(x) \le 1; \\ \frac{1}{1-\gamma} & \text{for } \mathcal{Z} = rQ_s(x) > 1; \end{cases} \quad (8)$$

which describes only leading twist contribution to the full BFKL kernel of Eq. (6). The lesson from this solution is very instructive: for $r^2 Q_s^2(x) \le 1$, the amplitude N satisfies the Dokshitzer-Gribov-Lipatov-Altarelli-Parisi (DGLAP) (BFKL) linear evolution equation with the boundary condition $N(Y;r;b) = N_0 = \text{Constant}$ for $r^2 = 1/Q_s^2(x)$, while for $r^2 Q_s^2(x) > 1$, we have a solution that has the form of Eq. (5). Using these general features of the solution we choose the model suggested in Ref. [27], which improves the earlier studies on this line [24,28]. In this model, the color-dipole–proton forward scattering amplitude is given by

$$N(Y;r;b) = \begin{cases} N_0\left(\frac{\mathcal{Z}}{2}\right)^{2(\gamma_s + (1/\kappa\lambda Y)\ln(2/\mathcal{Z}))} & \text{for } \mathcal{Z} = rQ_s(x) \le 2; \\ 1 - \exp(-A\ln^2(B\mathcal{Z})) & \text{for } \mathcal{Z} = rQ_s(x) > 2; \end{cases} \quad (9)$$

where the saturation scale $Q_s(x;b)$ (denoted by $Q_s(x)$ for brevity) is given by

$$Q_s(x;b) = \left(\frac{x_0}{x}\right)^{\lambda/2} \exp\left\{-\frac{b^2}{4(1-\gamma_{cr})B_{\mathrm{CGC}}}\right\}. \quad (10)$$

As we have already mentioned Eq. (9), as well as Eq. (10), has the form of the solution to the BK equation at a fixed QCD coupling. For $\mathcal{Z} < 1$, the effective anomalous dimension $\gamma_s + \frac{1}{\kappa\lambda Y}\ln(\frac{2}{\mathcal{Z}})$ with $\gamma_s = 1 - \gamma_{cr}$ follows from the BFKL (and DGLAP) equation in the vicinity of the saturation line (see Ref. [24] for the detailed derivation).

For the leading-order BFKL kernel with frozen QCD coupling, the parameters of Eqs. (9) and (10) have the following values

$$1 - \gamma_{cr} = 0.63; \qquad \lambda = \bar{\alpha}_s \frac{\chi(\gamma_{cr})}{1-\gamma_{cr}} = 4.88\bar{\alpha}_s; \qquad \kappa = \frac{\chi''(\gamma_{cr})}{\chi'(\gamma_{cr})} = 9.9. \quad (11)$$

The parameters A and B can be found from a matching of N and its logarithmic derivatives at $\mathcal{Z} = 2$, while N_0 and B_{CGC} remain fitting parameters.

Generally speaking, the model given by Eqs. (9) and (10) can be viewed as an approximation to the solution of the BK equation. However, because the b-dependent numerical solution to the BK equation is not yet available [23], we are doomed to resort to such an approximation. This model differs from other saturation models on the market since it apparently incorporates all known properties of the exact solution to the BK equation including the b dependence of the scattering amplitude (see Ref. [26]).

The advantage of Eqs. (9) and (10) is that these equations give the possibility to take into account the next-to-leading order (NLO) corrections. Two features of the nonlinear low-x equations can be calculated in the next-to-leading order using the kernel of the linear equation, the energy behavior of the saturation scale [6,29,30], and the behavior of the solution deeply in the saturation domain [26]. It has been shown that the NLO correction to the BFKL equation (and therefore BK equation) are large and it changes considerably the value of λ from $\lambda \approx 0.9$ to $\lambda \approx 0.3$ for $\bar{\alpha}_s = 0.2$ [31,32]. The value of γ_s in Eq. (9) is also affected by the NLO corrections as well as by the running QCD coupling [31–33]. It is, therefore, generally believed that the higher-order corrections to the NLO BK equation should be important. The actual calculation of higher-order corrections to these nonlinear evolution equations still remains as a challenge. Since the general behavior of the amplitude Eq. (9) will remain unchanged after inclusion of higher-order corrections, we effectively incorporate the

[2] Notice that here we assumed that the geometric scaling is also valid in the presence of impact-parameter dependence of the saturation scale. It should be stressed that the proof of the geometric-scaling behavior [25] could be easily generalized to the case of the scattering amplitude that depends on the impact-parameter b. In the analytical solution of Ref. [26], which gives the theoretical basis for the chosen parametrization of the dipole amplitude here, the b dependence is taken into account, therefore, this solution gives a theoretical example of the general proof.

higher-order corrections by taking the value of parameters λ, γ_s, N_0, x_0, and $B_{\rm CGC}$ obtained from a fit to the DIS data at low Bjorken x $x < 0.01$ [27]. Therefore, the saturation model that we use here gives also a good description of the HERA data at low x. In order to simulate the behavior of gluon density at large $x \to 1$, we product the unintegrated gluon density with $(1-x)^4$ as prescribed by quark counting rules [34]. This factor stems from the correct description of the HERA data on DIS.

B. Physical observables

The rapidity distributions of the minijets can be calculated using Eq. (1)

$$\frac{dN_{\rm minijet}}{d\eta} = h[\eta]\frac{1}{\sigma_{\rm nsd}}\int d^2p_T \frac{d\sigma}{dyd^2p_T}[\text{Eq. (1)}], \quad (12)$$

where η is the pseudorapidity and $h[\eta]$ is the Jacobian which takes account of the difference between rapidity y and the measured pseudorapidity η [13];

$$h(\eta, p_T) = \frac{\cosh\eta}{\sqrt{\frac{m_{\rm jet}^2+p_T^2}{p_T^2}+\sinh^2\eta}}, \quad (13)$$

where $m_{\rm jet}$ is the mass of minijet. One also has to express rapidity y in Eq. (1) in terms of pseudorapidity η. This relation is given by

$$y(\eta, p_T) = \frac{1}{2}\ln\left\{\frac{\sqrt{\frac{m_{\rm jet}^2+p_T^2}{p_T^2}+\sinh^2\eta}+\sinh\eta}{\sqrt{\frac{m_{\rm jet}^2+p_T^2}{p_T^2}+\sinh^2\eta}-\sinh\eta}\right\}. \quad (14)$$

The distribution Eq. (1) refers to the radiated gluons with zero mass while what is actually measured experimentally is the distribution of final hadrons. We, therefore, should make an assumption about hadronization of gluons which is an entirely nonperturbative process that has to be modeled in any approach due to lack of understanding of the confinement of quarks and gluon in QCD. However, it is well known that the general assumption about hadronization leads to the appearance of mass of the minijet, which is approximately equal to $m_{\rm jet}^2 \simeq 2\mu p_T$ (see Ref. [13]), where μ is the scale of soft interaction. The minijet mass $m_{\rm jet}$ effectively incorporates the nonperturbative soft prehadronization in the pseudorapidity space. Accordingly, one should also correct the kinematics every where in Eq. (1) due to the presence of a nonzero minijet mass, namely, replacing $p_T \to \sqrt{p_T^2+m_{\rm jet}^2}$ in x_1, x_2, and also in the denominator of $1/p_T^2$. One can see that Eq. (1) has infrared divergence at $p_T \to 0$ for the kinematic region $k_T \gg p_T$ when $m_{\rm jet} = 0$. In Ref. [13] it was suggested to integrate over $k_T \le p_T$. The reason is that such an integration reproduces the factorization formula at large $p_T \gg \mu$ for the DGLAP evolution. However, as we explained above it is more natural to replace p_T by $\sqrt{p_T^2+m_{\rm jet}^2}$ in Eq. (1), which consequently also regulates the denominator due to the presence of a nonzero minijet mass (the appearance of such mass is the general property of the hadronization processes).

In Eq. (12), we do not take into account the fragmentation of the produced gluon (minijet) into hadrons. We rely on the principle of Local Parton-Hadron Duality (LPHD) [35,36], namely, the form of the rapidity distribution will not be distorted by the jet decay, and only a numerical factor will differ the minijet spectrum from the hadron one. We believe that it is better to use the LPHD scheme than to deal with the fragmentation's functions for which we have no theoretical justifications at low p_T. It should be stressed that the same idea has been used in the KLN approach which describes the rapidity distribution of heavy-ion collisions data in a wide range of energies. This idea has also worked perfectly in e^+e^- annihilation into hadrons [35,36].

We should stress that the value of inelastic nonsinglet diffractive (NSD) cross section $\sigma_{\rm nsd}$ cannot be calculated in our approach and has to be taken from the soft-interaction models such as in Refs. [37,38]. The NSD cross section $\sigma_{\rm nsd}$ is defined as $\sigma_{\rm nsd} = \sigma_{\rm tot} - \sigma_{el} - \sigma_{sd} - \sigma_{dd}$, where σ_{el}, σ_{sd}, and σ_{dd} are the cross sections of elastic, single, and double diffraction, respectively. However, the experimental data on σ_{dd} is very limited [39]; σ_{sd} is measured with rather large errors [40,41], and, even for the total cross section $\sigma_{\rm tot}$ [41], we have two values at the Tevatron energies [42]. Therefore, we should stress that in this way we can only predict $d\sigma/dy$ rather than $dN_{\rm ch}/dy$. In order to overcome this problem, here we choose a different strategy: the physical meaning of $\sigma_{\rm nsd}$ in Eq. (12) is the area of interaction which can be calculated in our approach. Indeed, using Eq. (4), one can calculate the average impact parameter for the inclusive production of the minijet

$$\langle\vec{b}_{\rm jet}^2\rangle = \frac{\int\frac{d^2p_T}{p_T^2}\int d^2\vec{b}d^2\vec{B}d^2r_T(b^2+|\vec{b}-\vec{B}|^2)e^{i\vec{k}_T\cdot\vec{r}_T}\nabla_T^2N_G^{h_1}(y_1=\ln(1/x_1);r_T;b)\nabla_T^2N_G^{h_2}(y_2=\ln(1/x_2);r_T;|\vec{b}-\vec{B}|)}{\int\frac{d^2p_T}{p_T^2}\int d^2\vec{b}d^2\vec{B}d^2r_Te^{i\vec{k}_T\cdot\vec{r}_T}\nabla_T^2N_G^{h_1}(y_1=\ln(1/x_1);r_T;b)\nabla_T^2N_G^{h_2}(y_2=\ln(1/x_2);r_T;|\vec{b}-\vec{B}|)}. \quad (15)$$

The NSD cross section $\sigma_{\rm nsd}$ is then equal to the average interaction area up to a constant $\sigma_{\rm NSD} = M\pi\langle\vec{b}_{\rm jet}^2\rangle$. The prefactor M will be determined and discussed later. We should draw the reader's attention to the fact that such a picture for the inelastic cross section corresponds, in a sense, to the geometric-scaling behavior of the scattering amplitude. Indeed, the

high-density QCD deals with the partonic wave function of a fast hadron which describes a coherent system of partons (quarks and gluon). At high energy, the coherence of partons is destroyed during a short time and the partons, distributed as in the wave function, are produced. These partons contribute to the inelastic cross section. The elastic (diffractive) cross section corresponds to a rare event where the target does not destroy (or destroyed only partially) the coherence of the gluons in the wave function (see, for example, Ref. [43]). The geometric-scaling behavior, as well as the saturation phenomenon, in general, means that partons are distributed uniformly in the transverse plane in the wave function of a fast hadron in a such way that the wave function generates a uniform distribution of the produced partons after the interaction with the target. Therefore, the NSD (inelastic) cross section is proportional to the area occupied by partons. Actually, such a view on the inelastic cross section was suggested in the KLN approach [13] but for nucleus-nucleus and hadron-nucleus collision. Therefore, we generalize this approach to hadron-hadron scattering. We believe that if the LHC data at higher energy will support this idea, it will be a strong argument in favor of the saturation approach. The relation $\sigma_{\rm NSD} = \sigma_{\rm tot} - \sigma_{el} - \sigma_{sd} - \sigma_{dd}$ shows the obvious fact that the prediction for elastic and diffractive scattering are much more complicated and less transparent in the saturation approach. This is well-known fact, at least for diffractive production [44].

The average transverse momentum of the minijet is defined in the usual way:

$$\langle p_{\rm jet,T}\rangle = \int d\eta h[\eta] \int d^2p_T |p_T| \frac{d\sigma}{d\eta d^2p_T}[\text{Eq. (1)}] \Big/ \int d\eta h[\eta] \int d^2p_T \frac{d\sigma}{d\eta d^2p^T}[\text{Eq. (1)}] \tag{16}$$

The advantage of this quantity is that it can be calculated without usual uncertainties associated with the soft-interaction physics. The average transverse momentum of the jet can be directly related to the saturation scale via Eqs. (1), (9), and (16), and it has the following simple form at large $Q_s \gg m_{\rm jet}$

$$\langle p_{\rm jet,T}\rangle \propto \frac{Q_s}{\ln(Q_s^2/m_{\rm jet}^2 + 1) + \mathcal{Q}}, \tag{17}$$

where the parameter $\mathcal{Q}$ is of order of 1 and takes into account the contribution of integrals in Eq. (16) for $p_T > Q_s$.

In order to calculate the transverse momentum of hadrons, which is measured experimentally, we need to recall that $\vec{p}_{\rm hadron,T} = z\vec{p}_{\rm jet,T} + \vec{p}_{\rm intrinsic,T}$ which leads to

$$\langle p_{\rm hadron,T}\rangle = \sqrt{\langle z p_{\rm jet,T}\rangle^2 + \langle p_{\rm intrinsic,T}\rangle^2}, \tag{18}$$

where z is the fraction of energy of the jet carried by the hadron. $\langle p_{\rm intrinsic,T}\rangle$ is the average intrinsic transverse momentum of the hadron in the minijet. In other words, this is the transverse momentum of the hadron in the minijet that has only longitudinal momentum.

In the framework of the LHPD, the p_T spectrum of the produced hadron is equal to

$$\frac{dN_{\rm hadron}}{d^2p_T} = \int d\eta h[\eta] \frac{1}{\sigma_{\rm nsd}} \frac{d\sigma}{d\eta d^2p_{\rm jet,T}} \times [\text{Eq.(1)} \quad \text{with} \quad p_{\rm jet,T} = p_T/z], \tag{19}$$

where in the above p_T is the transverse momentum of the produced hadron.

In the CGC scenario, the gluon saturation scale is proportional to the density of partons (see Refs. [13,14]). The parton density is proportional to the multiplicity, and, therefore, we can use the following expression for the saturation momentum in the event with the multiplicity of the hadrons n:

$$Q_s(x) \to Q_s(n;x) = \frac{n}{\langle n\rangle} Q_s(x), \tag{20}$$

where $\langle n\rangle$ is the average multiplicity that has been measured in inclusive production without any selection related to multiplicity, and $Q_s(x)$ is the saturation scale for inclusive hadron production or $Q_s(n = \langle n\rangle; x)$. Using Eq. (17) again, one can relate the saturation scale at a given multiplicity to the average transverse momentum of the produced minijets at large $Q_s \gg m_{\rm jet}$,

$$\langle p_{\rm jet,T}; n\rangle \propto \frac{Q_s(n;x)}{\ln(Q_s^2(n;x)/m_{\rm jet}^2 + 1) + \mathcal{Q}}. \tag{21}$$

III. COMPARISON WITH THE EXPERIMENTAL DATA AND PREDICTION FOR HIGHER ENERGIES

In the derivation of the k_t factorization it was assumed that the strong-coupling α_s is a constant. As a generalization, in Eq. (1), we replace α_s by $\alpha_s(p_T)$, where p_T is the transverse momentum of the minijet, and in Eq. (2) we also replace $1/\alpha_s$ by $1/\alpha_s(Q_s(x_i))$, where $Q_s(x_i)$ is the saturation scale in hadron h_i. This seems to be the most natural way of introducing the running coupling, which still preserves the form of Eq. (4) apart from the overall factor outside of integrals, which now depends on kinematics. Indeed the inclusion of running strong coupling leads to improvement of our description. For the running strong-coupling α_s, we employ the same scheme as used by the KLN approach [13], namely, we use the leading-order running coupling with smooth freezing below the

virtuality $Q^2 \approx 0.8$ GeV^2, at the value of $\alpha_s^{\rm IR} \approx 0.5$. This is in accordance with many evidences from jet physics which indicates that the QCD coupling may stay reasonably small $\alpha_s^{\rm IR} = 0.4 \div 0.6$ in the infrared region [45].

The impact-parameter dependence in our formulation emerges from the employed impact-parameter dependent saturation scale, see Eqs. (9) and (10). In this model, the profile of the saturation scale in the proton is assumed to be a Gaussian. It is difficult to interpret the parameter $B_{\rm CGC}$ in Eq. (10) in terms of proton size due to the dipole size r and rapidity Y dependence of the anomalous dimension. Nevertheless, in order to have a intuitive picture, one may take $2B_{\rm CGC}$ as relative average squared transverse radius of the proton. The value of $B_{\rm CGC} = 7.5$ GeV^{-2} was obtained as a fit in order to describe the slope of t distribution of diffractive processes at HERA [27], which in turn fixes the normalization of the color-dipole–proton cross section. In Fig. 2 (right), we show the average impact parameter of jet $\langle \vec{b}^2_{\rm jet} \rangle$ from center of the hadrons. Notice that for obtaining $\langle \vec{b}^2_{\rm jet} \rangle$, the overall coefficient in Eq. (15) will be dropped out, and we are left with no free parameter. The $\langle \vec{b}^2_{\rm jet} \rangle$ is about $2.5B_{\rm CGC}$ and it slightly increases with energy.

The mass of minijet $m_{\rm jet}$ is proportional to the saturation scale $m^2_{\rm jet} \simeq 2\mu p_T$ [13] since the typical transverse momentum of the minijets is the saturation scale Q_s, and μ is the scale of soft interaction. The saturation scale in the CGC-b model Eq. (9) changes slowly with energy. For our interested range of energy considered in this paper at midrapidity $\eta = 0$ and $p_T = 1$ GeV for the central collisions $b = 0$, we have $Q_s \approx 0.6 \div 0.8$ GeV. Taking the scale of soft interaction equal to pion mass $\mu \approx m_\pi = 0.14$ GeV, we have $m_{\rm jet} \approx 0.4 \div 0.5$ GeV. We will first assume a fixed value for the minijet mass $m_{\rm jet} = 0.4$ GeV. To estimate the effect of the minijet mass, we will later consider a case with a different value for $m_{\rm jet}$.

In order to obtain the multiplicity distribution of hadrons in pp collisions from the corresponding minijets production cross section Eqs. (1) and (12), we have to fix some unknown parameters. First, based on the gluon-hadron duality, the rapidity distribution of hadron and radiated minijets can be different by a factor C. Second, although the k_t factorization incorporates the small-x evolution taking into account the higher-order gluon scatterings and nonlinear gluon recombination effects, nevertheless, given that we resort to a phenomenological color-dipole model, there might be still some extra contributions which are missed in our formulation. The discrepancy between the exact calculation and our formulation can be then effectively taken into account with a extra K factor. Finally, in order to obtain the charged-particle multiplicity, we should divide the minijet cross section with nonsinglet diffractive cross section which, as we already discussed, is obtained

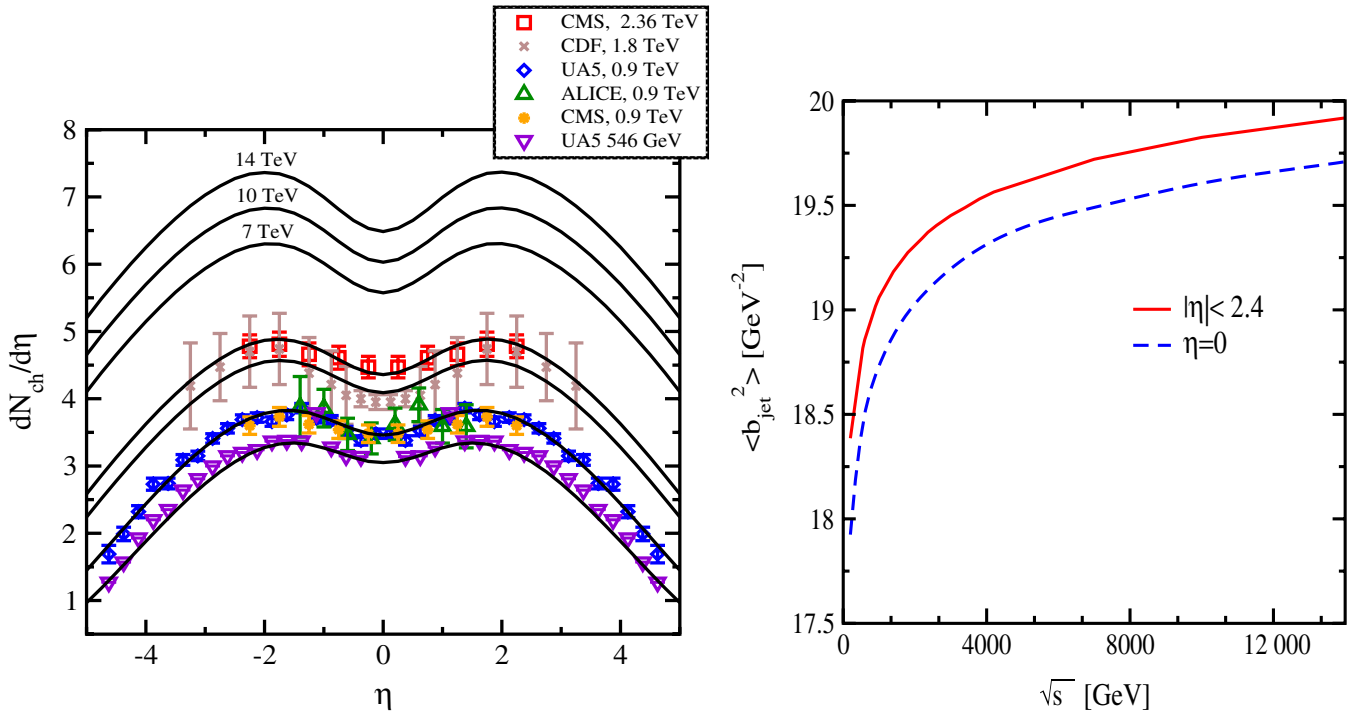

FIG. 2 (color online). Right: Shows the average impact parameter of the produced minijet $\langle b^2_{\rm jet} \rangle$ given by Eq. (15) as function of energy. Left: The comparison with the experimental data and prediction for $dN_{\rm ch}/dy$ using Eq. (12) with $\sigma_{\rm nsd} = M\pi\langle b^2_{\rm jet} \rangle$ for $|\eta| < 2.4$. The curves are normalized by data at $\sqrt{s} = 546$ GeV, see the text for the details. The experimental data are from Refs. [1,2,48]. The error bars on the UA5 and ALICE data points are statistical. We show only systematic errors for the CMS data points.

via $\sigma_{\rm nsd} = M\pi\langle\vec{b}^2_{\rm jet}\rangle$ with a new unknown dimensionless parameter M. Fortunately, these three unknown prefactors C, K, and M appear as a product and can be reduced to only one unknown parameter, which will be determined with a fit to the experimental data for the charged-particle multiplicity $\frac{dN_{\rm ch}}{d\eta}$ at midrapidity for the lowest energy considered here $\sqrt{s} = 546$ GeV. Therefore, we obtain $\frac{KC}{M} = 2.32$ at $\sqrt{s} = 546$ GeV. We assume that this overall normalization factor is energy independent. We expect that the energy dependence of the normalization factor to be proportional to $1 + O(1/\ln(1/x))$. Then, for higher energy $\sqrt{s} > 546$ GeV, we do not have any free parameters in our calculation, and our results may be considered as predictions of the model. Notice that we have employed a color-dipole model that its free parameters were obtained from a fit to the HERA data for $x_B < 0.01$ and $Q^2 \in [0.25, 45]$; therefore, our formulation is less reliable at lower energies (now used here). In Fig. 2 (left), we show the charged multiplicity distribution for pp collisions at various energies. Our model gives a good description of all available data for $\sqrt{s} \geq 546$ GeV, including the recently released data from ALICE [1], CMS [2], and ATLAS [3] at 0.9 and 2.36 TeV. We also show our predictions for the LHC energies at 7, 10, and 14 TeV. It is seen that as the energy increases, the peak of rapidity distribution at forward (backward) becomes more pronounced. This effect has been also observed in Ref. [46], where it was shown that the rapidity dependence of the invariant cross section, for both identified hadrons and direct photon, has a peak at forward rapidities, and this peak will be further enhanced by saturation effects [46].

In Fig. 3 (right), we show the charged-hadron pseudorapidity density in the central region $\eta = 0$ as a function of center-of-mass energy in pp collisions. Notice that since our prescription is valid only for the NSD interactions, we do not show the corresponding data for the inelastic event selection. We have also shown recently reported charged-particle pseudorapidity density from ALICE [4] at 7 TeV in $|\eta| < 1$ for inelastic collisions with at least one charged particle in that region (denoted by INEL > 0). Again, this point is out of the scope of our calculation, and we did not expect to explain it.

The main source of possible theoretical error in our calculation is due to the uncertainties associated with assuming a fixed value for the minijet mass for all energies and the uncertainty in value of energy-independent normalization factor KC/M obtained from a fit. The value of minijet mass is controlled by the saturation scale, and, as we already discussed, it can be $m_{\rm jet} \leq 0.65$ GeV for our interested range of energy here. Notice that the saturation scale in our model varies very slowly with energy. The upper limit of the theoretical uncertainty band in Fig. 3

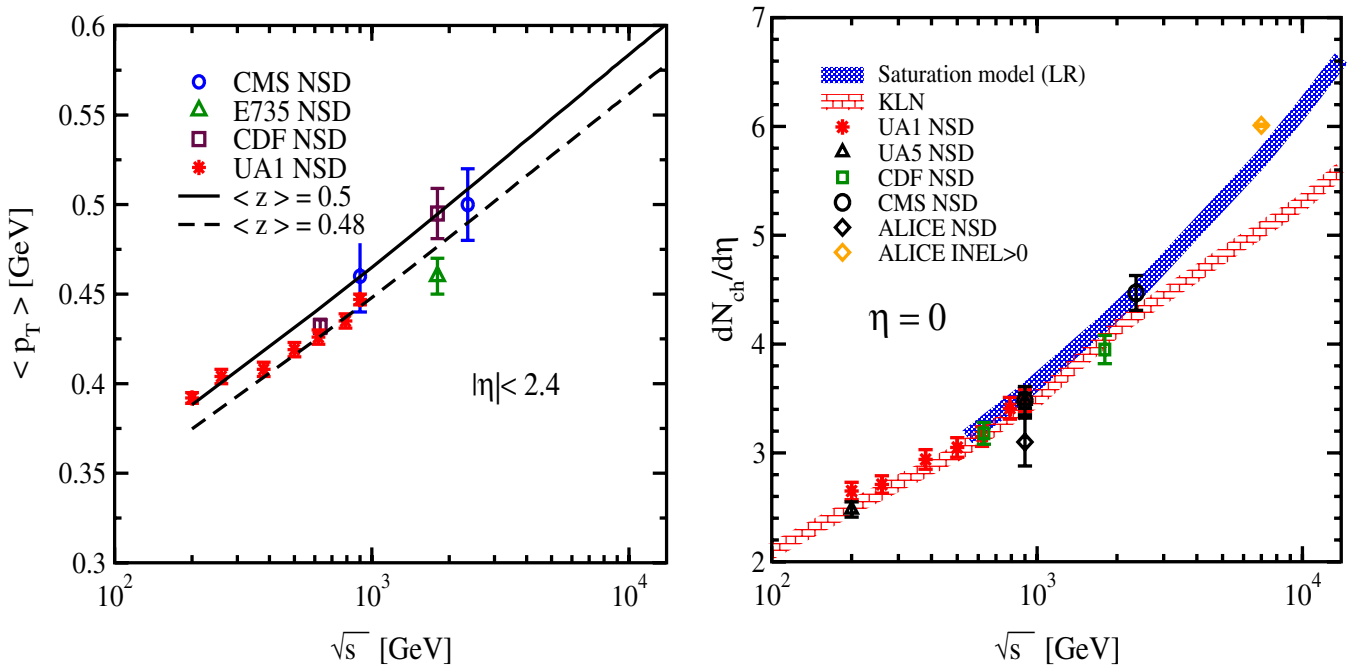

FIG. 3 (color online). Right: Energy dependence of the charged hadrons multiplicity in the central region of rapidity $\eta = 0$ in pp collisions. The theoretical curve (Saturation model LR) is our prediction coming from the saturation model for the NSD interactions. The band indicates about 2% theoretical error. The total theoretical uncertainties is less 6% at high energies (see the text for the details). We also show the KLN prediction [13] with the same error band as ours. Left: Our prediction for the energy dependence of the average transverse momentum of charged hadrons. The CMS data [2] points and the theoretical curves in the left panel are for $|\eta| < 2.4$. The experimental data are from Refs. [2,4,48–52]. The experimental error bars indicate systematic uncertainties.

(right) corresponds to a higher minijet mass $m_{\rm jet} = 0.5$ GeV. The experimental systematic and statistical errors in the data point taken for fixing the normalization also induce uncertainty in the value of prefactor KC/M obtained from a fit. This error is included in the band shown in Fig. 3 (right) and is less than the uncertainties coming from modeling the minijet mass. Overall, we expect less than 6% theoretical error in our calculation at higher energies.

Our approach improves saturation based (KLN approach) calculation [13] in several ways, including, using a correct relation between the unintegrated gluon density and the forward dipole-nucleon amplitude Eqs. (2) and (3) in the k_t factorization Eq. (1). As it is seen, this relation is not a simple Fourier transform of the dipole amplitude, which is commonly used in literature and also depends on the impact parameter. The impact-parameter dependence in these equations is not trivial and in principle should not be assumed as an overall factor. We then employed an impact-parameter dependent saturation model which was obtained from a fit to low Bjorken-x HERA data. In this sense, we had no freedom in modeling the saturation physics compared to the KLN approach. Moreover, since we have an impact-parameter formulation here, we could calculate the average relative interaction area at higher energies and, thereby, could also determine the relative increase of the NSD cross section. It should be recalled that in the KLN approach, the information about $\sigma_{\rm nsd}$ was taken from the models for the soft high-energy interactions, which is alien to the saturation approach. In both approaches, lower energy data for pp was used to fix the overall normalization factor. Therefore, we expect the discrepancies between our predictions and the KLN to be more pronounced at higher energies. This is, indeed, the case as it can be seen in Fig. 3 that the KLN prediction underestimates the multiplicity at higher energies.

The average transverse momentum of charge hadrons can be obtained from Eq. (18). In Eq. (18), the average intrinsic transverse momentum of hadron has a purely nonperturbative origin and is due to the finite-size effect of hadrons. We take $\langle p_{{\rm intrinsic},T}\rangle$ equal to the pion mass, the scale of soft-interaction $\mu = m_\pi$, throughout this paper. In order to obtain the average transverse momentum of charge hadrons, we need also to know the value of the average momentum fraction of minijets carried by the hadrons $\langle z\rangle$. It is seen from Fig. 3 (left) that an average value of $\langle z\rangle = 0.48 \div 0.5$ is remarkably able to describe the average transverse momentum of charge hadrons in a wide range of energies. Our theoretical curves and CMS data [2] are for the range $|\eta| < 2.4$. One may also estimate the value of $\langle z\rangle$ from the fragmentation functions, having in mind that the $\langle z\rangle$ for minijets in parton-hadron duality picture is not necessarily the same as the corresponding average of fragmentation momentum of the produced gluons in the parton model. Nevertheless, employing recently developed Albino-Kniehl-Kramer 2008 (AKK08) fragmentation functions [47] for charged hadrons production from a gluon, one obtains $\langle z\rangle = 0.5$, on average, over low p_T, within the range of $1 < p_T\ [\text{GeV}] \leq 2$ (AKK's fragmentation is valid only for $Q > 1$ GeV). In order to further test the validity of the value $\langle z\rangle \approx 0.5$ for the minijets, we show in Figs. 4 and 5 (top panel) our predictions obtained from Eq. (19) for the differential yield of charged hadrons in the range $|\eta| < 2.4$ and at various $|\eta|$ bins for $\sqrt{s} = 2.36$ TeV. The experimental data are recently reported from CMS collaboration [2]. It is seen that our results are in quite good agreement with experimental data. We recall again that the prefactor in Eq. (19) is the same as that which we already fixed with experimental multiplicity data at low-energy $\sqrt{s} = 546$ GeV at $\eta = 0$. Therefore, we have no free parameters in obtaining the theoretical curves in Figs. 4 and 5 (top). In Figs. 4 and 5 (top), we have also shown our predictions for $\sqrt{s} = 7$ and 14 TeV. The fact that our model reasonably works at low p_T (for $\sqrt{s} = 2.36$ TeV) is due to the fact that the saturation scale is rather large at low p_T; for $p_T \approx m_\pi$ we have $Q_s \approx 1$ GeV in the central rapidity region. Notice that the LPHD, in the simplified form that has been used here, is less reliable at higher p_T, and one should then somehow model the fragmentation of minijets into hadron.

In Fig. 5, there is seen a peculiar peak of the charged hadron's production rate at low $p_T \approx 0.2$ GeV. Actually, the appearance of such a peak is expected in our

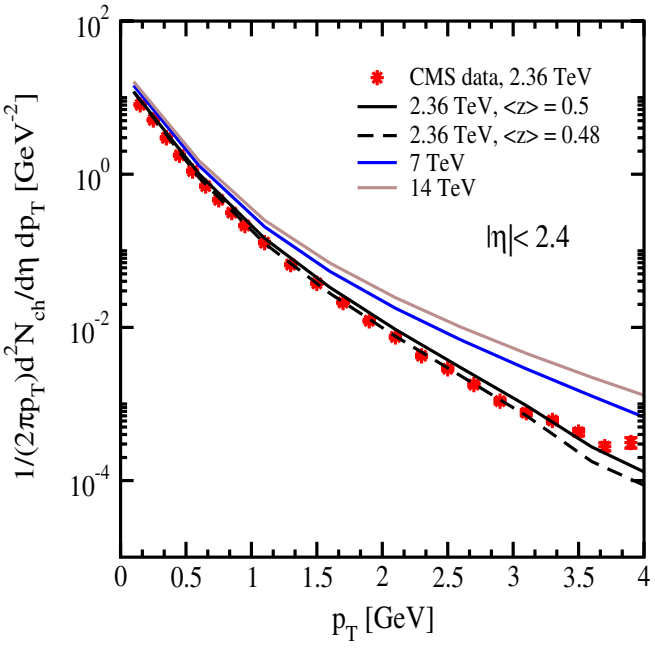

FIG. 4 (color online). The differential yield of charged hadrons for $|\eta| < 2.4$. The experimental data are from CMS [2] at 2.36 TeV for $|\eta| < 2.4$. We show also our theoretical predictions for 7 and 14 TeV with $\langle z\rangle = 0.5$ and $m_{\rm jet} = 0.4$ GeV. The experimental error bars shown are systematic and statistical errors added linearly.

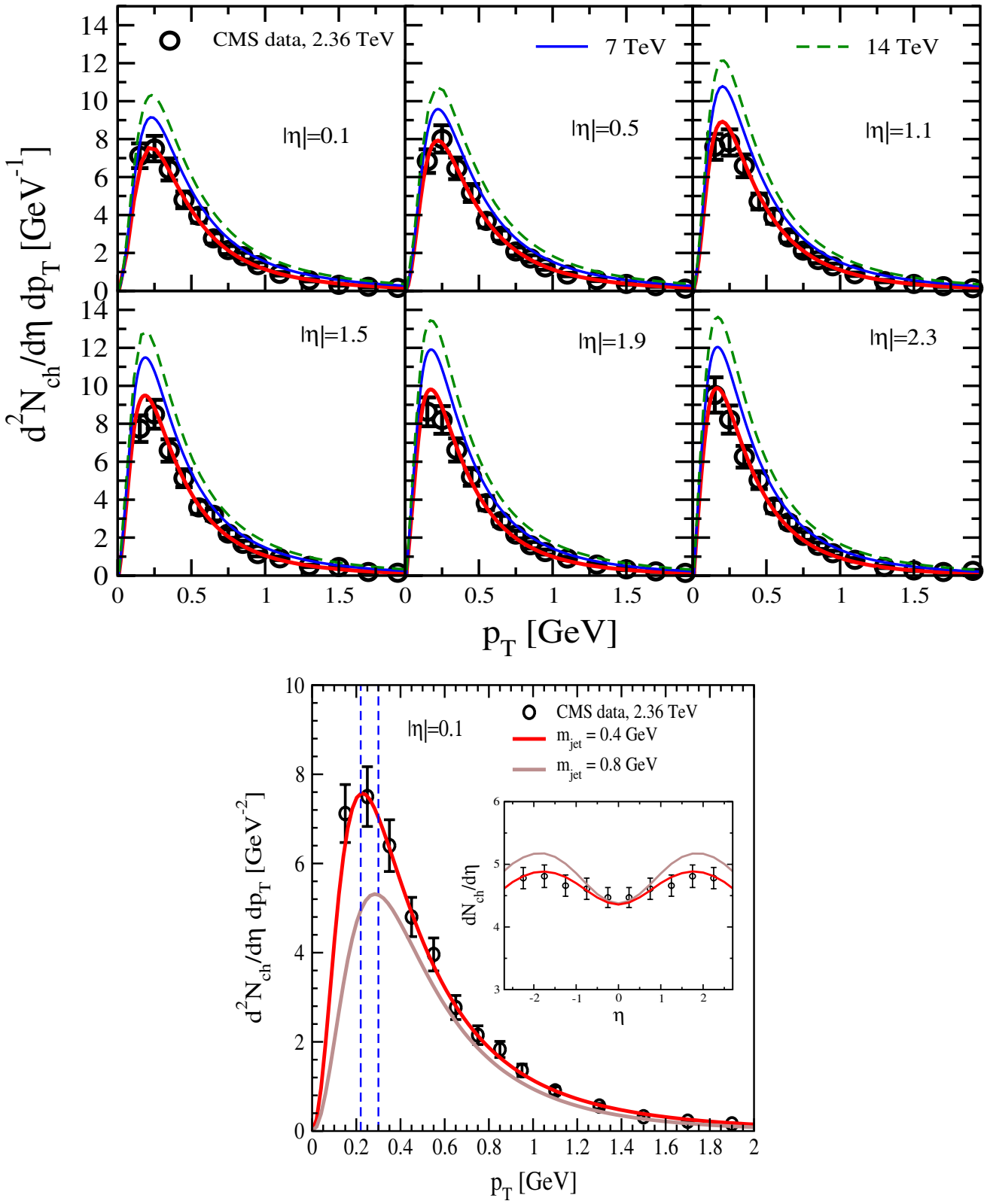

FIG. 5 (color online). Upper panel: The differential yield of charged hadrons in various $|\eta|$ bins for $\sqrt{s} = 2.36$ TeV. The experimental data are from CMS [2]. We also show our predictions for 7 TeV and 14 TeV with $\langle z \rangle = 0.5$ and $m_{\text{jet}} = 0.4$ GeV. The experimental error bars shown are systematic and statistical errors added linearly. Lower panel: The differential yield of charged hadrons for $|\eta| = 0.1$ for two different values of minijet masses m_{jet}. The inserted plot in the lower panel figure shows the charged hadrons multiplicity again for two values of m_{jet} for the same energy.

formulation. Notice that from Eq. (12), the differential yield of charged hadrons has a form $\frac{d^2N}{d\eta d p_T} \propto \frac{2\pi p_T}{p_T^2+\langle z\rangle^2 m_{\rm jet}^2}\mathcal{F}(x_1, x_2, p_T)$, where $\mathcal{F}$ is an analytic function. At $p_T = 0$ trivially, we have $\frac{d^2N}{d\eta d p_T} = 0$, for $p_T < m_{\rm jet}\langle z\rangle$, the spectra is a monotonically increasing function of p_T, and for $p_T > m_{\rm jet}\langle z\rangle$ it is decreasing due to the denominator. The position of the peak is then approximately at $p_T \simeq m_{\rm jet}\langle z\rangle \approx 0.2$ GeV, since we have $\langle z\rangle = 0.5$ and $m_{\rm jet} = 0.4$ GeV. This simple picture is consistent with the CMS experimental data [2] shown in Fig. 5 (top).

In order to see more clearly the effect of the minijet mass $m_{\rm jet}$, in Fig. 5 (down), we compare the differential yield of charged hadrons calculated with two different values for the minijet mass $m_{\rm jet} = 0.4$ and 0.8 GeV. We also show the multiplicity distribution in the inserted panel in Fig. 5. As we already pointed out, the mass of minijet is controlled by the saturation scale. Obviously, from the saturation scale in our model, $m_{\rm jet} = 0.8$ GeV is too large. Therefore, it is not surprising that the description of experimental data for both multiplicity and spectra worsened for such a large minijet mass. Nevertheless, it is obvious from Fig. 5 that the position of the peak moves to a higher p_T for a larger minijet mass. Note that the CMS experimental data [2] at $\sqrt{s} = 2.36$ TeV for the average transverse momentum of charged hadrons can be reproduced with $\langle z\rangle = 0.37$, when $m_{\rm jet} = 0.8$ GeV. Again, the position of the peak in spectra is consistent with simple formula $p_T \simeq m_{\rm jet}\langle z\rangle \approx 0.3$, in accordance with the full calculation shown in Fig. 5. Notice that in our model calculation, shown in Fig. 5 (top), the position of the peak persists at various rapidities bin (and energies) since we have taken a fixed $m_{\rm jet}$ for simplification. To conclude, a precise measurement of the differential yield of charged hadrons, at low p_T for higher energies at LHC, will provide valuable information about the minijet mass and its connection with the gluon saturation.

In Fig. 5 (top), we also showed our theoretical predictions for 7 and 14 TeV with a fixed $\langle z\rangle = 0.5$ and $m_{\rm jet} = 0.4$ GeV. As we already explained, due to the possible increase of minijet mass at higher energies, the position of peak may slightly move to higher p_T within $0.2 \leq p_T\ [\text{GeV}] \leq 0.3$ at $\sqrt{s} = 14$ TeV.

In Fig. 6, we show the average transverse momentum of charged hadrons as a function of the number of charged particles for events within the kinematic range $p_T > 500$ MeV. The experimental data are from ATLAS for $\sqrt{s} = 0.9$ TeV [3]. The saturation scale at various multiplicity is given by Eq. (20), where $\langle n\rangle$ can be conceived as a normalization and its value is taken to be the charged multiplicity at midrapidity $\eta = 0$ for a given center-of-mass energy [shown in Fig. 3 (right)]. In order to implement in our calculation the experimental kinematic constrain $p_T > 500$ MeV on the measured events, we impose that $\langle p_{\text{intrinsic},T}\rangle > 500$ MeV. The $\langle p_{\text{intrinsic},T}\rangle$ has a purely nonperturbative origin and can be of order of hadron mass.

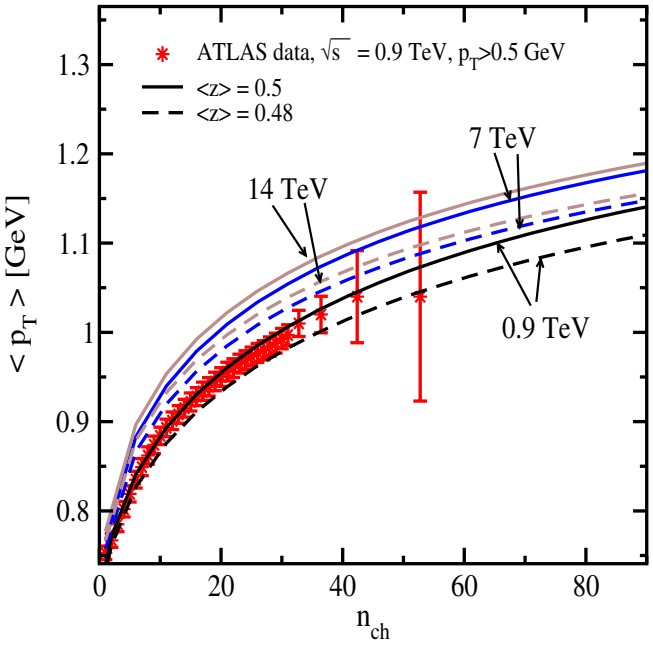

FIG. 6 (color online). The average transverse momentum of charged hadrons as a function of the number of charged particles for events with $n_{\rm ch} \geq 1$ within the kinematic range $p_T > 500$ MeV. The experimental data are from ATLAS for $\sqrt{s} = 0.9$ TeV and $|\eta| < 2.5$ [3]. The theoretical curves were obtained for $|\eta| = 0$ and with the same kinematic constraint $p_T > 500$ MeV at various energies for two values of $\langle z\rangle = 0.48$, 0.5 corresponding to the dashed and the solid lines, respectively. We only show the systematic experimental errors.

To this end, we take $\langle p_{\text{intrinsic},T}\rangle = (m_\rho + m_k)/2$, where the mass of ρ and k mesons are $m_\rho = 775$ MeV and $m_k = 497$ MeV, respectively. In Fig. 6, we show $\langle p_T\rangle$ for two values of $\langle z\rangle$. It is seen that our model is able to give a very good description of the ATLAS data. We have also shown in the same plot our predictions for the higher LHC energies.

The general behavior of the theoretical curves, shown in Fig. 3 (left) and Fig. 6 for the average transverse momentum of the produced hadrons, is in accordance with simple formulas given in Eqs. (17) and (21) showing a clear connection between the gluon saturation and the measured transverse momentum of charged hadrons.

IV. CONCLUSION

In high-density QCD, the main source of hadron production is the decay of gluon minijets with the transverse momentum of the order of the saturation scale. This viewpoint is based on the fact that the system of partons (gluons) creates a new state of matter, the so-called color glass condensate, in which the gluon density reaches the limited values of the order of $1/\alpha_s$ with new typical transverse momentum (the saturation scale). We developed a model that includes the gluon saturation and demon-

strated that this model is able to describe both the inclusive hadron production at high energies, including the first data from the LHC, and the deep inelastic scattering data from HERA in a unique fashion.

We predicted an increase of $dN_{\rm ch}/dy|_{\eta=0}$ mean transverse momentum and the multiplicity of produced charged hadrons with energy, which is in accordance with the first LHC data measured by ALICE [1,4], CMS [2], and ATLAS [3] Collaborations, see Figs. 2, 3, and 6. In the framework of high-density QCD, all these phenomena are closely related to the growth of the saturation momentum as a function of energy and of density of partons. It should be stressed that the other high-energy phenomenological approaches [5] cannot describe the dependence of the average transverse momentum of the produced hadron on energy and hadron multiplicities.

We showed that recently reported data by the CMS collaboration [2] on the differential yield of charged hadrons at low p_T for $\sqrt{s} = 2.36$ TeV reveal interesting information on the minijets production and its connection with the saturation. We showed that the appearance of a peak in differential yield of charged hadrons at low p_T is closely related to the minijet mass and the value of the saturation scale.

We provided various predictions for the upcoming LHC measurements at higher energies in pp collisions. We believe that this paper will be useful for the microscopic interpretation of the upcoming LHC data and will lead to a deeper understanding of the hadron interactions at high energy in the framework of QCD.

Concluding this paper, we would like to answer the question, what can be here considered as a possible signal of the saturation (CGC) which is not contaminated with the nonperturbative physics related to unknown confinement of quarks and gluon? The main nonperturbative parameter that we have to introduce is $m_{\rm jet}$. The rapidity distribution $dN_{\rm ch}/d\eta$ at $|\eta| < 1$ (Fig. 2), the p_t spectrum of hadron at low $p_T \leq m_{\rm jet}$, and the position of the maximum in $d^2N_{\rm ch}/d\eta dp_T$ (Fig. 5) depend on the value of $m_{\rm jet}$, and the success of our description indicates that we have chosen this parameter in a self-consistent way. However, the energy dependence of $dN_{\rm ch}/d\eta$ at $|\eta| \leq 3.5$ and the average value of the transverse-momentum $\langle p_T \rangle$ of hadrons, as well as the multiplicity dependence of $\langle p_T \rangle$ and the rapidity dependence of the maximum in $d^2N_{\rm ch}/d\eta dp_T$ for $|\eta| \leq 3.5$, are the typical consequences of the saturation approach, since the main contribution in the calculations of these observables is originated from the transverse momenta of the order of Q_s. Two factors determine the behavior of the observables at $|\eta| \geq 3.5$: $(1-x)^4$ suppression of the gluon densities in projectile, and the increase of the saturation momentum in the target. Since the $(1-x)^4$ factor reflects the well-known behavior of the structure function F_2 at large x, this factor will be the same in all other approaches, while the additional increase due to the energy dependence is a typical feature of the saturation approach. Notice also that at LHC energy $\sqrt{s} = 14$ TeV the contribution of $(1-x)^4$ correction of unintegrated gluon density within the rapidities region considered here (Fig. 2) is negligible, and at 7 TeV this contribution is less than 5%.

The above discussion shows that the comparison of our prediction with the high LHC energy data will be crucial for our approach. We are happy to make predictions before the experimental data from the LHC at high energy. We believe that if the coming data confirms our predictions this will be indeed a first important step toward discovery of the CGC phase of the matter at LHC. The fact that we had to introduce several phenomenological parameters reflects our lack of theoretical knowledge for quark and gluon confinement and cannot be overcome in any models. Our experience tells us that when the data for higher energies is published a lot of phenomenological models will appear, but the CGC (saturation) approach is the only one that gives the predictions. It has happened once for nucleus-nucleus scattering at RHIC, and we hope that the situation will repeat itself at the LHC.

The particle production scheme presented in this paper can be also applied to the calculation of inclusive hadron production in heavy-ion collisions at LHC. We are currently working on this problem and plan to report on this in the near future.

ACKNOWLEDGMENTS

We are thankful to Yuri Kovchegov for drawing our attention to Ref. [22]. This work was supported in part by Conicyt Programa Bicentenario PSD-91-2006 and the Fondecyt (Chile) Grants Nos. 1090312 and 1100648.

[1] K. Aamodt *et al.* (ALICE Collaboration), Eur. Phys. J. C **65**, 111 (2010); K. Aamodt *et al.* (ALICE Collaboration), arXiv:1004.3034.
[2] V. Khachatryan *et al.* (CMS Collaboration), J. High Energy Phys. 02 (2010) 041.
[3] G. Aad *et al.* (ATLAS Collaboration), Phys. Lett. B **688**, 21 (2010).
[4] K. Aamodt *et al.* (ALICE Collaboration), arXiv:1004.3514.
[5] E. Gotsman, E. Levin, and U. Maor, Phys. Rev. D **81**, 051501 (2010).
[6] L. V. Gribov, E. M. Levin, and M. G. Ryskin, Phys. Rep.

100, 1 (1983).
[7] A. H. Mueller and J. Qiu, Nucl. Phys. **B268**, 427 (1986).
[8] L. McLerran and R. Venugopalan, Phys. Rev. D **49**, 2233 (1994); **49**, 3352 (1994);**50**, 2225 (1994); **53**, 458 (1996); **59**, 094002 (1999).
[9] I. Balitsky, Nucl. Phys. **B463**, 99 (1996); Phys. Rev. D **60**, 014020 (1999).
[10] A. H. Mueller, Nucl. Phys. **B415**, 373 (1994); **B437**, 107 (1995).
[11] Y. V. Kovchegov, Phys. Rev. D **60**, 034008 (1999).
[12] J. Jalilian-Marian, A. Kovner, A. Leonidov, and H. Weigert, Phys. Rev. D **59**, 014014 (1998); Nucl. Phys. **B504**, 415 (1997); J. Jalilian-Marian, A. Kovner, and H. Weigert, Phys. Rev. D **59**, 014015 (1998); A. Kovner, J. G. Milhano, and H. Weigert, Phys. Rev. D **62**, 114005 (2000); E. Iancu, A. Leonidov, and L. D. McLerran, Phys. Lett. B **510**, 133 (2001); Nucl. Phys. **A692**, 583 (2001); E. Ferreiro, E. Iancu, A. Leonidov, and L. McLerran, Nucl. Phys. **A703**, 489 (2002); H. Weigert, Nucl. Phys. **A703**, 823 (2002).
[13] D. Kharzeev, E. Levin, and M. Nardi, Nucl. Phys. **A730**, 448 (2004); **A743**, 329 (2004); Phys. Rev. C **71**, 054903 (2005); D. Kharzeev and E. Levin, Phys. Lett. B **523**, 79 (2001); D. Kharzeev and M. Nardi, Phys. Lett. B **507**, 121 (2001).
[14] D. Kharzeev, E. Levin, and M. Nardi, Nucl. Phys. **A747**, 609 (2005).
[15] Y. V. Kovchegov and K. Tuchin, Phys. Rev. D **65**, 074026 (2002).
[16] M. A. Braun, Eur. Phys. J. C **48**, 501 (2006); Phys. Lett. B **483**, 105 (2000).
[17] C. Marquet, Nucl. Phys. **B705**, 319 (2005).
[18] A. Kovner and M. Lublinsky, J. High Energy Phys. 11 (2006) 083.
[19] E. Levin and A. Prygarin, Phys. Rev. C **78**, 065202 (2008).
[20] A. Kormilitzin, E. Levin, and A. Prygarin, Nucl. Phys. **A813**, 1 (2008).
[21] J. Bartels, M. Salvadore, and G. P. Vacca, J. High Energy Phys. 06 (2008) 032.
[22] M. A. Braun, arXiv:1003.1223.
[23] K. Golec-Biernat and A. M. Stasto, Nucl. Phys. **B668**, 345 (2003).
[24] E. Iancu, K. Itakura, and S. Munier, Phys. Lett. B **590**, 199 (2004).
[25] J. Bartels and E. Levin, Nucl. Phys. **B387**, 617 (1992); A. M. Stasto, K. J. Golec-Biernat, and J. Kwiecinski, Phys. Rev. Lett. **86**, 596 (2001); E. Iancu, K. Itakura, and L. McLerran, Nucl. Phys. **A708**, 327 (2002).
[26] E. Levin and K. Tuchin, Nucl. Phys. **B573**, 833 (2000).
[27] G. Watt and H. Kowalski, Phys. Rev. D **78**, 014016 (2008).
[28] H. Kowalski, L. Motyka, and G. Watt, Phys. Rev. D **74**, 074016 (2006).
[29] A. H. Mueller and D. N. Triantafyllopoulos, Nucl. Phys. **B640**, 331 (2002).
[30] S. Munier and R. B. Peschanski, Phys. Rev. D **70**, 077503 (2004); Phys. Rev. D **69**, 034008 (2004); Phys. Rev. Lett. **91**, 232001 (2003).
[31] D. N. Triantafyllopoulos, Nucl. Phys. **B648**, 293 (2003).
[32] V. A. Khoze, A. D. Martin, M. G. Ryskin, and W. J. Stirling, Phys. Rev. D **70**, 074013 (2004).
[33] J. L. Albacete and Y. V. Kovchegov, Phys. Rev. D **75**, 125021 (2007).
[34] S. J. Brodsky and G. R. Farrar, Phys. Rev. Lett. **31**, 1153 (1973); V. A. Matveev, R. M. Muradian, and A. N. Tavkhelidze, Lett. Nuovo Cimento Soc. Ital. Fis. **7**, 719 (1973).
[35] Y. L. Dokshitzer, V. A. Khoze, and S. I. Troian, J. Phys. G **17**, 1585 (1991).
[36] V. A. Khoze, W. Ochs, and J. Wosiek, arXiv:hep-ph/0009298; V. A. Khoze and W. Ochs, Int. J. Mod. Phys. A **12**, 2949 (1997), and reference therein.
[37] E. Gotsman, E. Levin, U. Maor, and J. S. Miller, Eur. Phys. J. C **57**, 689 (2008).
[38] M. G. Ryskin, A. D. Martin, and V. A. Khoze, Eur. Phys. J. C **54**, 199 (2008).
[39] A. A. Affolder *et al.* (CDF Collaboration), Phys. Rev. Lett. **87**, 141802 (2001).
[40] F. Abe *et al.* (CDF Collaboration), Phys. Rev. D **50**, 5535 (1994).
[41] K. Goulianos and J. Montanha, Phys. Rev. D **59**, 114017 (1999).
[42] F. Abe *et al.* (CDF Collaboration), Phys. Rev. D **50**, 5550 (1994).
[43] J. Bartels and H. Kowalski, Eur. Phys. J. C **19**, 693 (2001).
[44] Y. V. Kovchegov and E. Levin, Nucl. Phys. **B577**, 221 (2000).
[45] Y. L. Dokshitzer, arXiv:hep-ph/9812252; , Phil. Trans. R. Soc. A **359**, 309 (2001); G. P. Salam and D. Wicke, J. High Energy Phys. 05 (2001) 061.
[46] A. H. Rezaeian and A. Schäfer, Phys. Rev. D **81**, 114032 (2010); B. Z. Kopeliovich, E. Levin, A. H. Rezaeian, and I. Schmidt, Phys. Lett. B **675**, 190 (2009).
[47] S. Albino, B. A. Kniehl, and G. Kramer, Nucl. Phys. **B803**, 42 (2008).
[48] S. Eidelman *et al.* (Particle Data Group Collaboration), Phys. Lett. B **592**, 1 (2004).
[49] C. Albajar *et al.* (UA1 Collaboration), Nucl. Phys. **B335**, 261 (1990).
[50] G. J. Alner *et al.* (UA5 Collaboration), Z. Phys. C **33**, 1 (1986).
[51] F. Abe *et al.* (CDF Collaboration), Phys. Rev. D **41**, 2330 (1990); F. Abe *et al.* (CDF collaboration), Phys. Rev. Lett. **61**, 1819 (1988).
[52] A. M. Rossi *et al.*, Nucl. Phys. **B84**, 269 (1975).